Complex Structure of PDE3A–SLFN12 and Structure-based Molecular Glue Design for Apoptosis of Tumor Cells

Jie Chen
National Institute of Biological Sciences, Beijing https://orcid.org/0000-0001-8483-662X
Nan Liu
Tsinghua University
Dianrong Li
National Institute of Biological Sciences
Yuanxun Wang
National Institute of Biological Sciences, Beijing
Yuxing Sun
National Institute of Biological Sciences, Beijing
Qingcui Wu
National Institute of Biological Sciences, Beijing
Yinpin Huang
National Institute of Biological Sciences, Beijing
Hong-Wei Wang
Tsinghua University https://orcid.org/0000-0001-9494-8780
Niu Huang
National Institute of Biological Sciences, Beijing https://orcid.org/0000-0002-6912-033X
Xiangbing Qi (qixiangbing@nibs.ac.cn)
National Institute of Biological Sciences, Beijing https://orcid.org/0000-0002-7139-5164
Xiaodong Wang
National Institute of Biological Sciences, Beijing https://orcid.org/0000-0001-9885-356X

Article

Keywords: Protein-protein Interactions, Anagrelide, Cell Death, High-resolution Cryo-EM, Heterotetramer, Catalytic Domain, Targeted Protein Stabilization

Posted Date: March 30th, 2021

DOI: https://doi.org/10.21203/rs.3.rs-358451/v1

Version of Record: A version of this preprint was published at Nature Communications on October 27th, 2021. See the published version at https://doi.org/10.1038/s41467-021-26546-8.

Complex Structure of PDE3A–SLFN12 and Structure-based Molecular Glue Design for Apoptosis of Tumor Cells

Jie Chen[1,4], Nan Liu[2,4], Dianrong Li[1,4], Yuanxun Wang[1,4], Yuxing Sun[1,4], Qingcui Wu[1], Yinpin Huang[1], Hong-Wei Wang[2,*], Niu Huang[1,3,*], Xiangbing Qi[1,3,*], Xiaodong Wang[1,3,*]

[1]National Institute of Biological Sciences, 7 Science Park Road, Zhongguancun Life Science Park, Beijing 102206, China

[2]Ministry of Education Key Laboratory of Protein Sciences, Beijing Advanced Innovation Center for Structural Biology, Beijing Frontier Research Center for Biological Structures, School of Life Sciences, Tsinghua University, Beijing 100084, China

[3]Tsinghua Institute of Multidisciplinary Biomedical Research, Tsinghua University, Beijing, China

[4]These authors contributed equally: Jie Chen, Nan Liu, Dianrong Li, Yuanxun Wang, Yuxing Sun

[*]Correspondence should be addressed to H.-W.W. (hongweiwang@tsinghua.edu.cn), N.H. (huangniu@nibs.ac.cn), X.Q. (qixiangbing@nibs.ac.cn) or X.W. (wangxiaodong@nibs.ac.cn)

Abstract: Molecular glue is a class of small molecular drugs that mediate the protein-protein interactions. It can induce target proteins degradation or stabilization. Anagrelide, as a known phosphodiesterase 3A (PDE3A) inhibitor, is a drug used for the treatment of essential thrombocytosis. Here, we report Anagrelide induces cell death directly binding to PDE3A, which stabilizes protein Schlafen 12 (SLFN12). The high-resolution cryo-EM maps indicates that the interaction of PDE3A and SLFN12 exhibits a butterfly-like shape, to form a heterotetramer. Structure analysis showed that Anagrelide, as a new molecular glue, packs in a shallow pocket of PDE3A in the catalytic domain and the resulting modified interface binds SLFN12 through the short helix (E552-I558) of SLFN12. Based on the structure, we designed and synthesized the Anagrelide analogues with hydrophobic substitutes at 7-position. The *p*-tolyl substitution (compound A6) had the best improvement of around 20 folds, which IC_{50} is around 0.3 nM. Our studies revealed a new strategy to identify and develop a new molecular glue for targeted protein stabilization.

Introduction

PDE3A is phosphodiesterase that catalyze the hydrolysis of cyclic adenosine monophosphate (cAMP) and cyclic guanosine monophosphate (cGMP)(Francis et al., 2011). It contains three isoforms in cells, each with distinct N-terminal regulator domain and C-terminal catalytic domain(Manganiello et al., 1995). Biochemical experiments with truncation variants demonstrated

that the PDE3A catalytic domain is sufficient for the hydrolysis of cAMP and cGMP(Hung et al., 2006). Studies have shown that PDE3 enzymes are involved in regulation of cardiac and vascular smooth muscle contractility(Movsesian and Kukreja, 2011). Molecules that inhibit PDE3 were originally investigated for the treatment of heart failure, like Cilostazol(Zhang et al., 2002), Milrinone(Zhang et al., 2002), Anagrelide(Wang et al., 2005). All of these FDA-approved drugs are functioned by PDE3A's hydrolyzing cAMP or cGMP.

However, in 2016, de Waal and their colleagues found that DNMDP can induce cell death by mediating the interaction of PDE3A and SLFN12, but without depending on the hydrolysis function of PDE3A(de Waal et al., 2016). Subsequently, D. Li.et al. (2019) demonstrated that an estrogen-related hormone can induce interaction between PDE3A and SLFN12, and showed that this interaction stabilizes SLFN12 in cells. The elevated SLFN12 binds to ribosome, thereby blocking the continuous protein translation, include Bcl-2 and Mcl-1, whose decrease triggers apoptosis cell death(Li et al., 2019). R. An. et al. (2019) showed that a PDE3A inhibitor (Anagrelide) induces interaction between PDE3A and SLFN12 and activates death signaling(An et al., 2019). Y. Ai.et al. (2020) revealed that a natural product (Nauclefine) also can induce cell death by promoting the PDE3A-SLFN12 interaction (Ai et al., 2020). These multiple lines of evidence together indicate that some apparently promiscuous binding site on PDE3A can accommodate small molecules with quite diverse chemical structures. However, the nature of their binding with PDE3A remains unclear; indeed, it is not known whether these small molecules act to enhance the PDE3A-SLFN12 interaction allosterically (via binding and induction of conformational change(s)) or whether they may function as a "molecular glue" to facilitate PDE3A-SLFN12 complex formation.

Anagrelide (Agrylin/Xagrid), is an imidazoquinazoline derivative that was used as an inhibitor of platelet aggregation (Fleming and Buyniski, 1979). It also was useful for the treatment of essential thrombocytosis (also known as essential thrombocythemia) in patients with chronic myeloproliferative disorders(Abe Andes et al., 1984). Anagrelide induces the complexation of PDE3A and SLFN12 and prevents the SLFN12 degradation, and therefore increases the levels in living cells. However, the precise molecular mechanism by which Anagrelide brings about the interaction between PDE3A and SLFN12 and the interaction details of this molecule are still unknown.

We herein disclosed the complex structure with Anagrelide as s a new molecular glue to induce the complexation of PDE3A and SLFN12 and form a heterotetramer. Based on the complex structure and the details of the binding motif, we designed and synthesized a variety of Anagrelide analogs. The cell-death induction activity of these analog was explored. The results of this study provide detailed insights into the mechanism of action of Anagrelide with the complex of PDE3A-SLFN12; the structural data provide information on the basis for broad clinical drug development in terms of molecular glue strategy.

RESULTS

1. Anagrelide-mediated cell death depends on PDE3A and SLFN12.

Estrogen-related hormones induce PDE3A-dependent cell death (Li et al., 2019), doing so in a manner independent of PDE3A's enzymatic activities. Our screening efforts using an FDA-approved compound library against PDE3A showed that Anagrelide induces cell death in a dose-dependent manner. We later found that this Anagrelide-induced cell death can be blocked by co-treatment with PDE3 inhibitors including cilostazol (Cilo) and Trequinsin (Treq) (Figure 1A). Based

on this, we speculated that Anagrelide-induced cell death may depend on PDE3A, an idea we pursued by treating HeLa (WT, PDE3A$^{-/-}$, SLFN12$^{-/-}$) cells with different concentrations of Anagrelide for 48 h. Anagrelide induced HeLa cell death in WT but not PDE3A$^{-/-}$ of SLFN12$^{-/-}$ cells (Figure 1B). SLFN12 protein increased in response to Anagrelide treatment. Consistently, no SLFN12 increase was observed in the absence of PDE3A (Figure 1C).

We also expressed a SLFN12-Flag fusion protein in SLFN12$^{-/-}$ cells; after Anagrelide treatment for 12h, western blotting with an antibody against PDE3A showed that i) co-IP of PDE3A and SLFN12 required Anagrelide treatment and SLFN12 protein increased (Figure 1D, lane 2) and ii) co-treatment with the PDE3 inhibitor Treq completely blocked the physical interaction between PDE3A and SLFN12, SLFN12 protein level didn't increased (Figure 1D, lane 3), indicating that the observed increase in SLFN12 protein level is dependent on the Anagrelide-induced PDE3A-SLFN12 interaction.

2. Cryo-EM structures of SLFN12 and PDE3A complexes formed in the presence of multiple molecular glue compounds

Recalling that multiple small molecules with highly distinct chemical structures can promote the PDE3A-SLFN12 interaction and induce cell death (*e.g.*, Anagrelide and DNMDP), we conducted structural studies to elucidate how these compounds exert these functions at the atomic level. Specifically, we treated HeLa (SLFN12$^{-/-}$)-SLFN12(K213R)-HA-3×Flag cells with Anagrelide or DNMDP for 24 h, followed by lysis and purification of PDE3A-SLFN12 complexes using Flag-HA tandem pull-down. We then performed single-particle cryo-EM reconstruction to determine the structures of the SLFN12-PDE3A complexes (Figure S1 and Table S1) induced by the presence of Anagrelide (Figure 2A; Figure S2a and c; 3.4-Å resolution), and DNMDP (Figure S2b and d; 3.2-Å). The main chains could be unambiguously traced in these structures, and most side chains could be nicely assigned, enabling us to successfully build the atomic models. Moreover, the densities of ions were visible in our structures, exemplified by the Zn^{2+} ion in SLFN12's zinc finger (Figure S3) and Mg^{2+} ions in the PED3A catalytic sites (Figure S4).

We found that both complex structures exhibited the same butterfly-like shape, appearing as dimers of SLFN12-PDE3A heterodimers, containing full-length SLFN12 and the C terminal region of PDE3A (*i.e.*, the catalytic domain). Notably, since both SLFN12 and PDE3A were constructed at full length, the absence of N terminal density of PDE3A in our structures was likely due to the extreme flexibility. In our dimer of PDE3A-SLFN12 heterodimer structures, we identified two hydrogen-bond networks formed at dimeric interfaces, located on the opposite sides of the complex (Figure 2B).

PDE3A's C terminal region contains the catalytic domain for hydrolysis of cGMP/cAMP (Figure 2C) (Hung et al., 2006); our model indicted that this region adopts a similar 3D conformation in PDE3A as its isoform PDE3B (Scapin et al., 2004). The catalytic site was clearly resolved, comprising the H756, H836, D837, and D950 residues, chelating two metal cations. H752 is known to function as a proton donor during cGMP/cAMP hydrolysis in phosphodiesterase; this residue was also positioned nearby the catalytic site in our PDE3A model.

SLFN12 is readily conceptualized as having an N-terminal and a C-terminal domain (Figure 2D). The N terminus of SLNF12 is composed of two lobes connected by a bridging domain, together generating a U-shaped "valley" with a ~17-Å mouth. Two positively-charged patches responsible for RNA binding are located at the entrance of the valley (residues K35, K38, K39, R46 and R213,

R217, K219). C terminal density was absent in previously published structures of SLFN family proteins (Yang et al., 2018). Our complex structures indicated that SLFN12's C-terminal region is folded as a separate domain, extending away from the N-terminal region via a flexible loop connection. In our complex structure, a short helix (residues E552-I558) in the C-terminal region projects out from the main SLFN12 body (Figure 2D), reaching PDE3A and thus forming the heterodimeric interface between PDE3A and SLFN12, which is consistent with our truncation variant experiments that residues comprising the short helix (E552-I558) of SLFN12 are essential for the interaction with PDE3A.

Although Anagrelide and DNMDP are structurally diverse molecules, our structure indicated that both of them occupied the same binding pocket of PDE3A (Figure 2E-G), termed the substrate-binding pocket, and took the similar interaction manner with PDE3A-SLFN12 complex, with their hydrophilic head anchored inside and hydrophobic tail outside (Figure 2E-G). Hydrogen-bond interacting networks are formed between PDE3A and the head of Anagrelide, as well as DNMDP. Taking Anagrelide as an example (Figure 2E-F), the H-bond network involves the oxygen atom of Anagrelide and the nitrogen in the side chain of H961, and the nitrogen atoms of Anagrelide with the side chain of Q1001 (Figure 2F). Additionally, Anagrelide is stacked with the phenyl ring in the side chain of PDE3A's F1004. SLFN12's helix552-558 is positioned at the pocket mouth, and the side chains of its L554, I557 and I558 residues comprise a highly hydrophobic moiety for interactions with their hydrophobic tail, together with L910, I951, I968, F972, L1000 and F1004 of PDE3A (Figure 2F-G). These hydrophobic interactions illustrate how these two molecules function in connecting PDE3A and SLFN12 as the molecule glue: molecule with one side at the pocket of PDE3A tightly anchored helix552-558 of SLFN12 by hydrophobic interaction.

Under normal cellular conditions, the SLFN12 protein is kept at a very low level based on ubiquitin-mediated protein degradation (Li et al., 2019). The formation of a PDE3A-SLFN12 complex would likely interfere the ubiquitination-related factors loading onto SLFN12, due to the steric effect, thus preventing degradation and thereby promoting accumulation of SLFN12 in cells.

3. The Anagrelide-induced PDE3A-SLFN12 interaction depends on PDE3A's catalytic domain and SLFN12's C-terminal region

Based on the structure analysis, we next conducted cell-death-induction assays with truncation variants of PDE3A expressed in HeLa ($PDE3A^{-/-}$) cell to help characterize Anagrelide's interaction site. PDE3A truncation aa669-1102 (CD-1) supported Anagrelide-induced cell death, whereas a truncation aa679-1141 (CD-2) residues (which include known catalytic domain residues) did not induce cell death (Figure 3A). Moreover, PDE3A truncations (CD-1 and CD-2) were stably transfect in HeLa($SLFN12^{-/-}$)-HA-3×Flag cells, immunoprecipitation experiments showed that PDE3A's CD-1 domain interacts with SLFN12 in the presence of Anagrelide, whereas PDE3A's CD-2 domain does not interact (Figure 3B), indicating that catalytic domain of PDE3A is binding domain with SLFN12.

Recall that multiple small molecules with highly distinct chemical structures can directly binds PDE3A with the same sites, including T751, H961, L1000, Q1001, F1004. To test the importance of these sites in compounds-induced cell death, Myc-tagged wild-type (WT) PDE3A and variants bearing amino acid mutants (T751A, H961A, L1000A, Q1001A, F1004A) were stably transfect in HeLa cells lacking its endogenous PDE3A. All of the variants didn't rescue the cell death under Anagrelide treatment (Figure 3C), indicating that these sites are essential for Anagrelide-PDE3A

binding.

We also expressed three different C-terminal truncation variants of SLFN12 in SLFN12$^{-/-}$ HeLa cells (SLFN12(aa1-550)-Flag, SLFN12(aa1-560)-Flag, or SLFN12(aa1-570)-Flag). Then we analyzed immunocomplexes which had formed by 12 h after Anagrelide treatment, a time point before cell death has fully manifested. The SLFN12(aa1-560) and SLFN12(aa1-570) variants can each interact with PDE3A in the presence of Anagrelide; however, the SLFN12(aa1-550) variant does not bind PDE3A (Figure 3D). Based on the elevated SLFN12 can execute cell death directly, we also monitored cell death using methyl blue staining after 72 h without Anagrelide treatment. All of the truncations of SLFN12 have the function to induce cell death (Figure 3E), indicating that the interaction domain is in the C terminal and residues aa550-560 of SLFN12 is essential for interaction between PDE3A and SLFN12, just like the structure shows.

4. Structure-guided optimization of Anagrelide led to A6 with significant increased activity.

Our Cryo-EM structure clearly indicated that Anagrelide acts as a molecular glue to form a stable ternary complex with PDE3A and SLFN12 (Figure 4A). We noted that Anagrelide's acyl guanidine moiety form hydrogen bonds with PDE3A's Q1001 and H961 residues, which is critical for PDE3A binding(Venuti et al., 1987). Anagrelide's phenyl moiety engaged in *pi-pi* stacking with PDE3A's F1004, which was demonstrated as an essential role in PDE3-ligand binding(Scapin et al., 2004). We also observed that the 7-Cl group of Anagrelide engage in hydrophobic interactions of both proteins, specifically with PDE3A's T844, F972, and L910 and with SLFN12's I557 and I558 in SLFN12 (Figure 4B). We noted a significant decrease in activity in cell-death-induction assays with an Anagrelide analogue from which the 7-Cl group was removed (Table S2, compound A14).

Based on our PDE3A-SLFN12 complex structure and this cell-death-induction assay data, we speculated that the space present at the Anagrelide-tail binding area may enable optimization to achieve superior molecular glue performance. Pursing this, we used the OpenGrowth (Cheron et al., 2016) program to automatically sample the potential substitutions on the Anagrelide's phenyl ring to differentially interact with PDE3A and SLFN12; we subsequently used a MM-GB/SA rescoring protocol(Huang et al., 2006a; Huang et al., 2006b) to rank the candidate Anagrelide analogues based on calculated binding energy, which delineates the contributions to the binding affinity (Table S3). Compared to Anagrelide, more than one third of the hypothetical Anagrelide analogs that have hydrophobic substitution at the 7-position interact more favorably with SLFN12, especially the analogs with 7-phenyl ring (Figure 4B).

We then synthesized and tested a variety of Anagrelide analogs with hydrophobic substitutions at the 7-position, including aromatic rings or aliphatic chains (Table S2). Encouragingly, cell-death-induction assay showed that the induction activity of these compounds was increased significantly comparing with the original Anagrelide. An analogue with the *p*-tolyl substitution (compound A6) conferred the most potent induction activity—around a 22- fold improvement over Anagrelide (Figure 4D-4E) (Table S2). Analogs with acyclic aliphatic chains showed improvements over Anagrelide but not to the same extent as A6. Bulkier substitutions like the naphthalene of A11, the *p*-ethyl phenyl of A20, the *p*-propyl-phenyl of A21, and the *p*-isopropyl-phenyl of A22 led to lower induction activity, indicating that the space between Anagrelide and I557 and I558 is limited and only suitable for medium sized ring systems. Explicit modelling of the PDE3A-SLFN12-A6 indicated that the *p*-tolyl substitution indeed forms additional hydrophobic interactions with SFLN12's I557 and I558 residues, which is the key for its molecular glue property (Figure 4C).

Discussion

Here, we have known multiple small molecules with highly distinct chemical structures can promote the PDE3A-SLFN12 interaction and induce cell death (e.g., estradiol, DNMDP, Anagrelide, Nauclefine). Structure analysis showed that PDE3A possess a stable binding pocket that can accommodate these molecules. These small molecules binding PDE3A allows PDE3A to recruit cell death executor SLFN12 by interacting with SLFN12's helix552-558.

Both SLFN12- and PDE3A-family proteins have been reported to exist as homodimers (Aravind et al., 2003; Goyal et al., 2016; Scapin et al., 2004), with known oligomerization contributions from the conserved residues we detected in the hydrogen-bond networks formed at the dimeric interaction interfaces of the dimer of SLFN12-PDE3A heterodimer structures. Specifically, at the PDE3A dimeric interface, hydrogen bonds are formed between the side chains of one PDE3B monomer's Y859, N860, and D861 residues with the main-chain oxygen of L858 and the side chains of the N867 and R898 residues of the second PDE3B monomer (Figure 2B left). For the SLFN12 dimeric interface, hydrogen bonds are formed between one SLFN12 monomer's K128, K135, T132, and T199 residues with the L88, S84, E80, and E25 residues of the second SLFN12 monomer (Figure 2B right).

Our structures added more evidences to support the idea that SLFN12 might function as dimeric state *in vivo*. Interestingly, we found that the valley diameter in SLFN12 (Figure 2D) was much smaller than that in SLFN13 (~23 Å) (Figure S5). Given that SLFN13 is known to recognize and cleave double-stranded regions of transfer RNAs (tRNA) and ribosomal RNAs (rRNA) (Yang et al., 2018), the narrower valley diameter suggests that SLFN12 may recognize distinct RNA substrates compared to SLFN13.

Importantly, we found that the Anagrelide and DNMDP likely shared the same binding pocket of cyclic nucleotides in PDE3A, based on the sequence conservation analysis and comparison with the structure of its isoform, PDE3B (Scapin et al., 2004). Therefore, the occupation by Anagrelide or DNMDP of PDE3A would preclude the binding of cyclic nucleotides, thus inhibiting its hydrolysis activity.

We also synthesized several hydrophilic Anagrelide analogs, including a phenol (compound A13), a carboxyl of phenyl (compound A16), and a pyridinyl (compound A10) (Figure 4F): the decreased induction activities we detected for these analogs supported the calculation results that hydrophobic groups at 7- position was suitable for molecular glue design. We also synthesized the hydrophobic analogs at other positions of the phenyl ring, however, only the 7- derivatives showed distinguished affinity. Further hydrophobic substituent modification at the 8-position based on compound A6 (compound A15) (Figure 4G) resulted in reduced induction activities; these results indicated a large ortho-group might disrupt the *p*-tolyl interaction with SFLN12's I557 and I558. However, the less-flexible *o*-tolyl (A18) counterparts of A6, which is not as active as A6, suggested that the spatial configuration of the tolyl ring is crucial for better induction activity. In conclusion, based on the complex structure of PDE3A-SLFN12-Anagrelide, the Anagrelide analogs with superior molecular glue performance were developed and the therapeutical potential was demonstrated via the PDE3A-SLFN12 induced cell-death assay.

Methods

Cells and Plasmids. HeLa, HEK293T, HeLa (PDE3A$^{-/-}$), HeLa (SLFN12$^{-/-}$), HeLa-PDE3A(aa669-

1108)-myc, HeLa-PDE3A(aa679-1141)-myc cells were cultured in DMEM (GIBCO) with 10% FBS (Invitrogen) and 1% penicillin and streptomycin at 37 °C with 5% CO_2. psPAX2, PMD2.G, pWPI constructs were kept in our lab. Myc-tagged truncated PDE3A(aa669-1108 and aa679-1141) and HA-3×Flag tagged truncated SLFN12(aa1-550, aa1-560, aa1-570) were constructed in pWPI. Point mutations were generated using a Quikchange Site-Directed Mutagenesis Kit.

Cell viability assay. Cell viability assays were performed by measuring the cellular ATP level using a Cell Titer-Glo Luminescent Cell Viability Assay kit (Promega) according to the manufacturer's instructions. The luminescence intensity was read by a microplate reader (Tecan GENios).

Western blotting. Cell pellets were collected and re-suspended in lysis buffer (100mMTris-HCl, pH 7.4, 100mMNaCl, 10% glycerol, 1% Triton X-100, 2 mM EDTA, Roche complete protease inhibitor set, and Sigma phosphatase inhibitor set) or NativePAGETM sample buffer (Thermo Fisher), incubated on ice for 30 min, and centrifuged at 20,000 x g for 30 min. The supernatants were collected for western blotting analysis. The antibodies used in this research were: PDE3A antibody from Bethyl Laboratories (1:1000, Cat# A302-740A); anti-Rabbit-HRP antibody from Sigma-Aldrich (1:5000, Cat# A0545); anti Mouse-HRP antibody from Sigma-Aldrich (1:5000, Cat# A9044); MYC-HRP antibody from MBL (1:1000, M-047-7); Flag-HRP antibody from Sigma-Aldrich (1:10,000, Cat#A8592); Actin-HRP antibody from MBL (1:50,000, Cat# PM053-7) and anti-GAPDH-HRP antibody from MBL (1:50,000, Cat# M171-1).

Transfections. HeLa (SLFN12-/-) cells were transfected with plasmids using Lipofectamine 3000 (Thermo Fisher) following the manufacturer's instructions.

Virus Packaging. To prepare the virus, HEK293T cells in the 10-cm dish were transfected with 15 mg of pWPI-PDE3A(WT and mutants)-Myc, pWPI-SLFN12 (WT and mutants)-HA-3×Flag, construct DNA together with 11.25 mg of psPAX2 and 3.75 mg of pMD2.G. Eight hours after transfection, the media were changed to high-serum DMEM (20% FBS with 25mM HEPES). Another 40 hours later, the media were collected and centrifuged at 3,000 rpm for 10 min. The supernatant was filtered through a 0.22-mm membrane and aliquots of 15 mL were stored at -80℃.

Methylene blue staining. Cells were seeded in six-well plates. After treatment, cells were washed with PBS and stained with 1.5% methylene blue dissolved in 50% ethanol for 10 min at room temperature. Cells were then washed with PBS and photos were taken.

Flag-HA Tandem Pull-Down. The cells were cultured on 10 cm dishes and grown to confluence. Cells at 90% confluence were washed once with PBS and harvested by scraping and centrifugation at 800×g for 5 min. The harvested cells were washed with PBS and lysed for 30 min on ice in the lysis buffer. Cell lysates were then spun down at 12,000×g for 20 min. The soluble fraction was collected, and the protein concentration was determined by Bradford assay. Next, 1 mg of extracted protein in lysis buffer was immunoprecipitated overnight with anti-Flag or anti-Myc affinity gel (Sigma-Aldrich) at 4℃. The immunoprecipitates were washed three times with lysis buffer. The beads were then eluted with 0.5 mg/ml of the corresponding antigenic peptide for 4 hr or directly boiled in 1% SDS loading buffer.

Cryo-EM specimen preparation. A drop of 3.5 μl solution containing SLFN12-PDE3A complex with compounds was pipetted onto EM grid (Au 300mesh, R1.2/1.3) coated by homemade graphene film, which had been previously glow-discharged in a low-energy plasma cleaner (Harrick PDC-32G) for 12s to be hydrophilic. After loading sample, the grid was transferred into an FEI Vitrobot (Thermo Fisher Scientific) with the humidity of 100% and the temperature of 8 ℃, and blotted by filter papers (TED PELLA) for 2s with -2 force. Afterwards, the grid was plunge-frozen into liquid

ethane and stored at liquid nitrogen.

Cryo-EM Data collection and processing. Cryo-EM datasets were collected on a Titan Krios (Thermo Fisher) with an accelerated voltage of 300 kV, equipped with a CS corrector and a Gatan K3 summit detector. The movies were automatically acquired by the AutoEMation software written by Dr. Jianlin Lei at Tsinghua University with a total dose of 50 $e^-/Å^2$, every of which contained dose-dependently fractionated 32 frames. We collected 2,526 micrographs for Anagrelide-induced complex, and 2,128 micrographs for DNMDP-induced complex, respectively. For data processing, we firstly applied MotionCor2 (Zheng et al., 2017) to correct the beam-induced motion of individual frames and used Relion3.1 (Scheres, 2012) to perform the following 3D reconstruction. The CTF values of these motion-corrected micrographs were determined by CTFFIND4 algorithm (Rohou and Grigorieff, 2015). After that, particles were autopicked and extracted in Relion3.1, which were then pooled into 2D classification for selecting good particles. After 3D classification and refinement with C2 symmetry, we obtained the structures of Anagrelide- and DNMDP-induced PDE3A-SLFN12 complex at 3.4-Å and 3.2-Å resolution, respectively, estimated by the Fourier Shell Correction (FSC)=0.143 cutoff criteria. Particle numbers used for the final reconstructions were 82,930 for Anagrelide-induced complex, and 203,914 for DNMDP-induced complex.

Model Building. We built the atomic model of PDE3A based on a previously reported model of PDE3B (Scapin et al., 2004) and for the N-terminal region of SLFN12 based on a reported model of SLFN13 (Yang et al., 2018). A C-terminal model of SLFN12 was generated by SWISS-MODEL (Waterhouse et al., 2018), with manual adjustment in COOT (Emsley and Cowtan, 2004). The complex models were finally refined in Phenix (Afonine et al., 2018). We used UCSF Chimera (Pettersen et al., 2004) to analyze the structural files and generate figures in the manuscript

Computational details of molecular glue design. OpenGrowth v1.0.1 was used to automatically generate Anagrelide analogues at position 7(Cheron et al., 2016). The option of GROWTH_MODE in parameter file was set to FOG, the list of fragments of Fragments-OpenGrowth-413 was used during the growth. The option of MAX_FRAGMENTS in parameter file was set to 3. Totally 200 newly generated poses (totally 44 unique ligands) from OpenGrowth program were submitted to MM-GB/SA rescoring using Protein Local Optimization Program(Jacobson et al., 2002) the details of rescoring can be found in previously published paper(Huang et al., 2006a; Huang et al., 2006b).

Chemistry. All reactions were carried out under an atmosphere of nitrogen in flame-dried glassware with magnetic stirring unless otherwise indicated. Commercially obtained reagents were used as received. Solvents were dried by passage through an activated alumina column under argon. Liquids and solutions were transferred via syringe. All reactions were monitored by thin-layer chromatography with E. Merck silica gel 60 F254 pre-coated plates (0.25 mm). 1H and 13C NMR spectra were recorded on Varian Inova-400 or 500 spectrometers. Data for 1H NMR spectra are reported relative to CDCl3 (7.26 ppm), CD3OD (3.31 ppm), or DMSO-d6 (2.50 ppm) as an internal standard and are reported as follows: chemical shift (δppm), multiplicity (s = singlet, d = doublet, t = triplet, q = quartet, sept = septet, m = multiplet, br = broad), coupling constant J (Hz), and integration. Data for 13C NMR spectra are reported relative to CDCl3 (77.23 ppm), CD3OD (49.00 ppm) or DMSO-d6 (39.52 ppm) as an internal standard and are reported in terms of chemical shift (δ ppm). Samples preparation and purity analysis were conducted on Waters HPLC (Column: XBridge C18, 5μm, 19 x 150 mm) with 2998PDA and 3100MS detectors, and Waters UPLC (Column: BEH C18, 1.7μm, 2.1 x 50 mm) with PDA and SQD MS detectors, using ESI as ionization. HRMS data were obtained on a Thermo Q Exactive.

All new compounds were synthesized as indicated in details in schemes in the supplementary information. Compounds A2 were synthesized according to the same synthetic route as compound A1 using different starting materials 3-fluoro-2-chlorobenzaldehyde. Di-substituted compounds A3, A4, A6-A14, A16, A18-A22 were synthesis using Suzuki coupling reaction from A1. Compounds A5 were synthesized according to the same synthetic route as compound A17 using different starting materials 3,4,5-trichloroaniline. Tri-substituted compound A15 was synthesized using Suzuki coupling reaction from A17. A14 was the by-product of Suzuki coupling reaction for di-substituted compounds.

Reporting summary. Further information on research design is available in the Nature Research Reporting Summary linked to this article.

Data availability

The cryo-EM maps of Anagrelide- and DNMDP-induced PDE3A-SLFN12 complexes have been deposited in the EMDB under accession number EMD-31103 and EMD-31104, respectively, and the coordinates in the PDB with PDB ID: 7EG0 and 7EG1, respectively.

Reference

Abe Andes, W., Noveck, R.J., and Fleming, J.S. (1984). Inhibition of platelet production induced by an antiplatelet drug, anagrelide, in normal volunteers. Thromb Haemost *52*, 325-328.

Afonine, P.V., Poon, B.K., Read, R.J., Sobolev, O.V., Terwilliger, T.C., Urzhumtsev, A., and Adams, P.D. (2018). Real-space refinement in PHENIX for cryo-EM and crystallography. Acta Crystallogr D Struct Biol *74*, 531-544.

Ai, Y., He, H., Chen, P., Yan, B., Zhang, W., Ding, Z., Li, D., Chen, J., Ma, Y., Cao, Y.*, et al.* (2020). An alkaloid initiates phosphodiesterase 3A-schlafen 12 dependent apoptosis without affecting the phosphodiesterase activity. Nat Commun *11*, 3236.

An, R., Liu, J., He, J., Wang, F., Zhang, Q., and Yu, Q. (2019). PDE3A inhibitor anagrelide activates death signaling pathway genes and synergizes with cell death-inducing cytokines to selectively inhibit cancer cell growth. Am J Cancer Res *9*, 1905-1921.

Aravind, L., Iyer, L.M., and Anantharaman, V. (2003). The two faces of Alba: the evolutionary connection between proteins participating in chromatin structure and RNA metabolism. Genome Biol *4*, R64.

Cheron, N., Jasty, N., and Shakhnovich, E.I. (2016). OpenGrowth: An Automated and Rational Algorithm for Finding New Protein Ligands. J Med Chem *59*, 4171-4188.

de Waal, L., Lewis, T.A., Rees, M.G., Tsherniak, A., Wu, X., Choi, P.S., Gechijian, L., Hartigan, C., Faloon, P.W., Hickey, M.J.*, et al.* (2016). Identification of cancer-cytotoxic modulators of PDE3A by predictive chemogenomics. Nat Chem Biol *12*, 102-108.

Emsley, P., and Cowtan, K. (2004). Coot: model-building tools for molecular graphics. Acta Crystallogr D Biol Crystallogr *60*, 2126-2132.

Fleming, J.S., and Buyniski, J.P. (1979). A potent new inhibitor of platelet aggregation and experimental thrombosis, anagrelide (BL-4162A). Thromb Res *15*, 373-388.

Francis, S.H., Blount, M.A., and Corbin, J.D. (2011). Mammalian cyclic nucleotide phosphodiesterases: molecular mechanisms and physiological functions. Physiol Rev *91*, 651-690.

Goyal, M., Banerjee, C., Nag, S., and Bandyopadhyay, U. (2016). The Alba protein family: Structure

and function. Biochim Biophys Acta *1864*, 570-583.
Huang, N., Kalyanaraman, C., Bernacki, K., and Jacobson, M.P. (2006a). Molecular mechanics methods for predicting protein-ligand binding. Phys Chem Chem Phys *8*, 5166-5177.
Huang, N., Kalyanaraman, C., Irwin, J.J., and Jacobson, M.P. (2006b). Physics-based scoring of protein-ligand complexes: enrichment of known inhibitors in large-scale virtual screening. J Chem Inf Model *46*, 243-253.
Hung, S.H., Zhang, W., Pixley, R.A., Jameson, B.A., Huang, Y.C., Colman, R.F., and Colman, R.W. (2006). New insights from the structure-function analysis of the catalytic region of human platelet phosphodiesterase 3A: a role for the unique 44-amino acid insert. J Biol Chem *281*, 29236-29244.
Jacobson, M.P., Kaminski, G.A., Friesner, R.A., and Rapp, C.S. (2002). Force Field Validation Using Protein Side Chain Prediction. The Journal of Physical Chemistry B *106*, 11673-11680.
Li, D., Chen, J., Ai, Y., Gu, X., Li, L., Che, D., Jiang, Z., Li, L., Chen, S., Huang, H.*, et al.* (2019). Estrogen-Related Hormones Induce Apoptosis by Stabilizing Schlafen-12 Protein Turnover. Mol Cell *75*, 1103-1116 e1109.
Manganiello, V.C., Taira, M., Degerman, E., and Belfrage, P. (1995). Type III cGMP-inhibited cyclic nucleotide phosphodiesterases (PDE3 gene family). Cell Signal *7*, 445-455.
Movsesian, M.A., and Kukreja, R.C. (2011). Phosphodiesterase inhibition in heart failure. Handb Exp Pharmacol, 237-249.
Pettersen, E.F., Goddard, T.D., Huang, C.C., Couch, G.S., Greenblatt, D.M., Meng, E.C., and Ferrin, T.E. (2004). UCSF chimera - A visualization system for exploratory research and analysis. J Comput Chem *25*, 1605-1612.
Rohou, A., and Grigorieff, N. (2015). CTFFIND4: Fast and accurate defocus estimation from electron micrographs. J Struct Biol *192*, 216-221.
Scapin, G., Patel, S.B., Chung, C., Varnerin, J.P., Edmondson, S.D., Mastracchio, A., Parmee, E.R., Singh, S.B., Becker, J.W., Van der Ploeg, L.H.*, et al.* (2004). Crystal structure of human phosphodiesterase 3B: atomic basis for substrate and inhibitor specificity. Biochemistry *43*, 6091-6100.
Scheres, S.H. (2012). RELION: implementation of a Bayesian approach to cryo-EM structure determination. J Struct Biol *180*, 519-530.
Venuti, M.C., Jones, G.H., Alvarez, R., and Bruno, J.J. (1987). Inhibitors of cyclic AMP phosphodiesterase. 2. Structural variations of N-cyclohexyl-N-methyl-4-[(1,2,3,5-tetrahydro- 2-oxoimidazo[2,1-b]quinazolin-7-yl)-oxy]butyramide (RS-82856). J Med Chem *30*, 303-318.
Wang, G., Franklin, R., Hong, Y., and Erusalimsky, J.D. (2005). Comparison of the biological activities of anagrelide and its major metabolites in haematopoietic cell cultures. Br J Pharmacol *146*, 324-332.
Waterhouse, A., Bertoni, M., Bienert, S., Studer, G., Tauriello, G., Gumienny, R., Heer, F.T., de Beer, T.A.P., Rempfer, C., Bordoli, L.*, et al.* (2018). SWISS-MODEL: homology modelling of protein structures and complexes. Nucleic Acids Res *46*, W296-W303.
Yang, J.Y., Deng, X.Y., Li, Y.S., Ma, X.C., Feng, J.X., Yu, B., Chen, Y., Luo, Y.L., Wang, X., Chen, M.L.*, et al.* (2018). Structure of Schlafen13 reveals a new class of tRNA/rRNA- targeting RNase engaged in translational control. Nat Commun *9*, 1165.
Zhang, W., Ke, H., and Colman, R.W. (2002). Identification of interaction sites of cyclic nucleotide phosphodiesterase type 3A with milrinone and cilostazol using molecular modeling and site-directed mutagenesis. Mol Pharmacol *62*, 514-520.

Zheng, S.Q., Palovcak, E., Armache, J.P., Verba, K.A., Cheng, Y., and Agard, D.A. (2017). MotionCor2: anisotropic correction of beam-induced motion for improved cryo-electron microscopy. Nat Methods *14*, 331-332.

Acknowledgements. We thank Dr. John Snyder for critically reading and editing the manuscript. We thank Dr. Jianlin Lei, Dr. Xiaomin Li, Dr. Fan Yang, Xiaofeng Hu and Cuixia Hu at the Cryo-EM and High-Performance Computation platforms of Tsinghua University Branch of the National Protein Science Facility, for the technical support in cryo-EM data collection and analysis. This work was supported by an institutional grant from the Chinese Ministry of Science and Technology and by Beijing Municipal Commission of Science and Technology.

Author contributions. J.C, N.L, D.L and Y.H were the key contributor in designing and conducting majority of the experiments. X.W, X.Q, J.C and D.L conceived and directed the project. X.W, X.Q, J.C, N.L and D.L wrote the manuscript. N.L. and H.W. performed the cryo-EM reconstruction and model building of PDE3A-SLFN12 complex. X.Q, Y.S and Q.W designed and synthesized the compound (A1-A22). N.H and Y.W performed the computational design and molecule scoring based on the complex structure of PDE3A/SLFN12.

Competing interests.
A provisional patent application (PCT/CN2021/082486) has been filed for the application of Anagrelide analogs and use thereof.

Figures

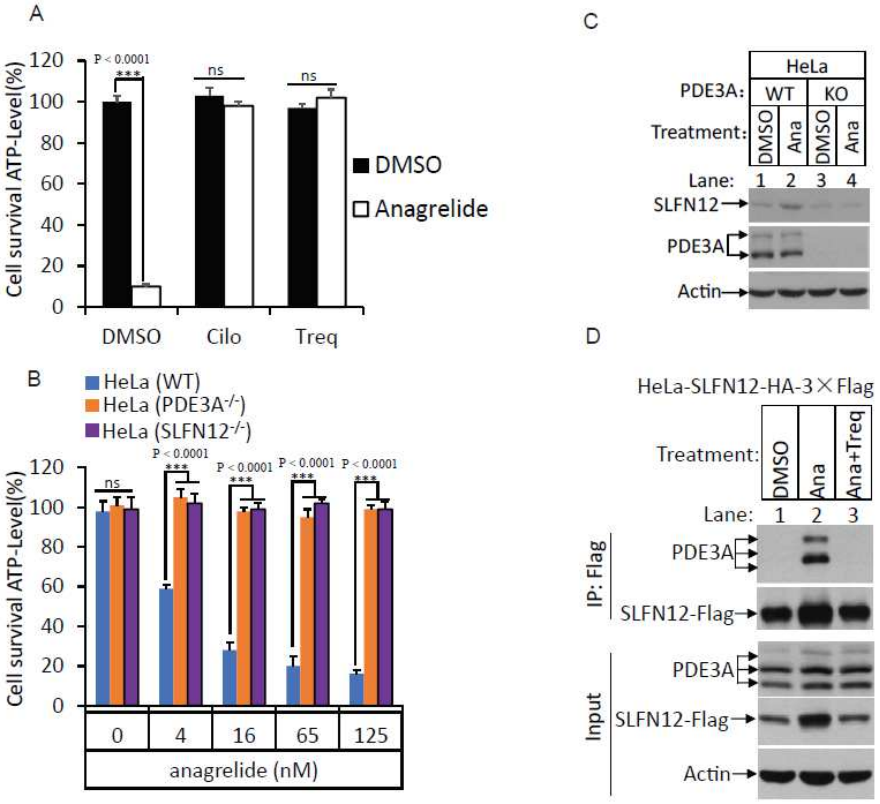

Figure 1. Anagrelide-mediated cell death depends on PDE3A and SLFN12

(A) HeLa cells were treated with the indicated stimuli for 36 hours. Cell viability was determined by measuring ATP levels. The data are represented as the mean ± SD of triplicate wells. Identical concentrations of Anagrelide (100 nM), Cilostazol (1 μM) and Trequinsin (25 nM) were used in subsequent experiments unless otherwise stated.

(B) HeLa (WT), HeLa (PDE3A$^{-/-}$) and HeLa (SLFN12$^{-/-}$) cells were treated with Anagrelide with the indicated concentration for 36 hours. Cell viability was determined by measuring ATP levels. The data are represented as the mean ± SD of triplicate wells.

(C) HeLa (WT and PDE3A$^{-/-}$) cells were treated with the indicated stimuli for 12 hours. The lysates were analyzed by immunoblotting using SLFN12 and PDE3A antibody.

(D) HeLa-SLFN12-HA-3×Flag cells were treated with the indicated stimuli for 12 hours. SLFN12 was immunoprecipitated using anti-Flag resin. The immunocomplexes and lysates were analyzed by immunoblotting using antibodies as indicated.

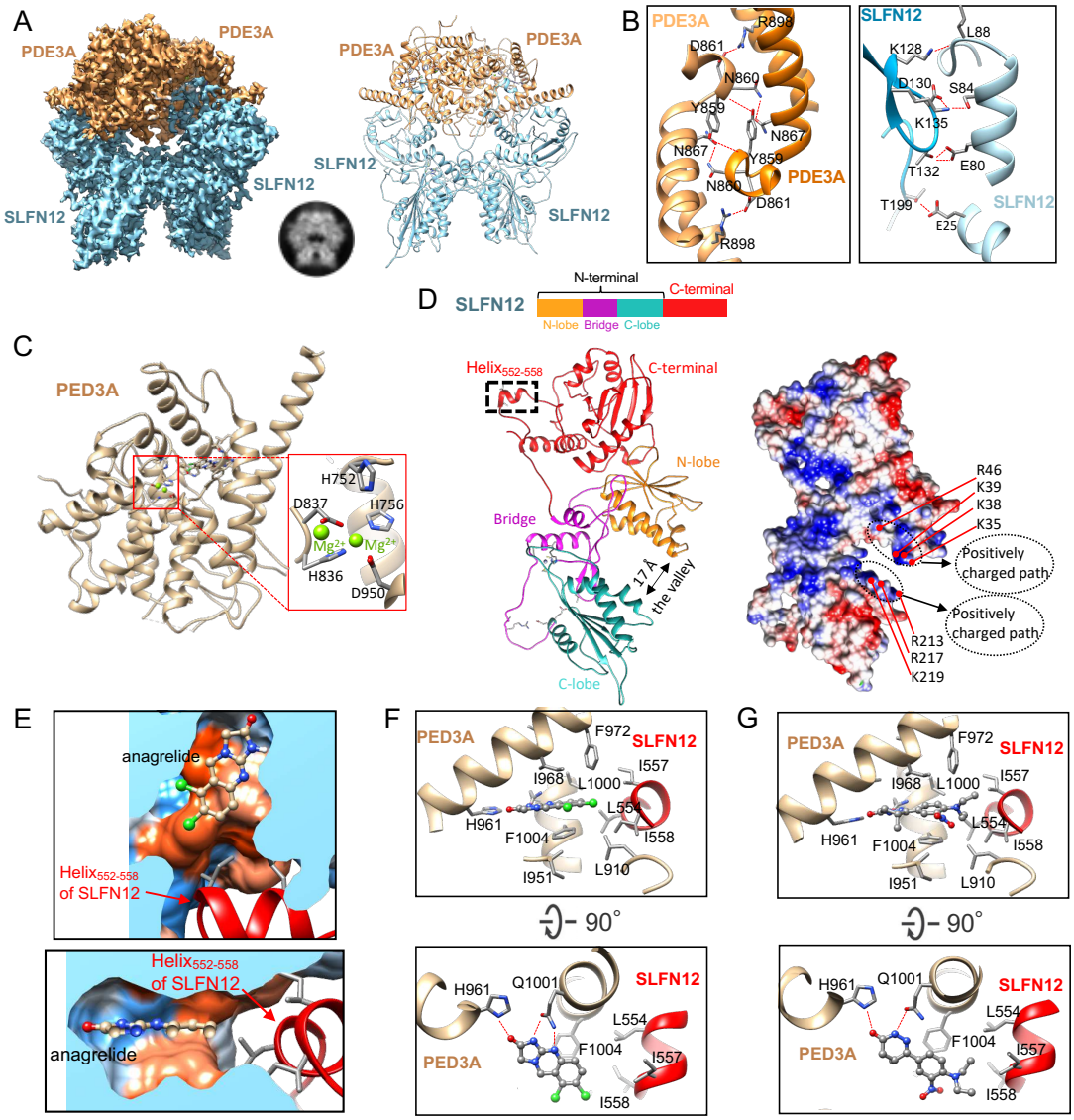

Figure 2. Cryo-EM analysis of Anagrelide- and DNMDP-induced PDE3A-SLFN12 complexes. (A) The cryo-EM reconstruction of Anagrelide-induced PDE3A-SLFN12. Left, the cryo-EM density with PDE3A colored in sandy brown and SLFN12 in light blue. Right, the corresponding atomic model. A selected image from the 2D classification was also displayed, demonstrating the butterfly-like shape. (B) The dimeric interaction interfaces of PDE3A (left) and SLFN12 (right). Hydrogen bonds were labelled by red dotted lines. (C) The model of C terminal of PDE3A. The zoom-in image of Mg^{2+} ions binding site was indicated by the red box. Residue H752 of PDE3A was folded close to the two Mg^{2+} ions. (D) Left was the model of SLFN12, divided to two domains, the N-terminal and C-terminal domains. The N-terminal domain consisted of two lobes and a bridge motif, forming a U-shaped valley with a diameter of ~17 Å. Right was the electrostatic surface potentials of SLFN12 in the same view to the left model, colored from red (negative) to blue (positive). The positively charged amino acids located at the valley mouth were indicated, forming two positively charged paths, responsible for RNA binding. (E) Tow zoom-in views of anagrelide-binding pocket in PDE3A-SLFN12 complex. Upper view was parallel to the plane of anagrelide, while the below view was perpendicular to anagrelide plane. PDE3A was shown as hydrophobicity surface, colored from orange red (hydrophobic) to blue (hydrophilic). The helix552-558 of Slfn12

was colored in red ribbon. (F) Anagrelide-binding site in PDE3A-SLFN12 complex. Anagrelide was anchored at the binding pocket by forming hydrogen-bond network with H961 and Q1001 of PDE3A and hydrophobic interaction with helix$_{552\text{-}558}$ of SLFN12. (G) DNMDP-binding site in PDE3A-SLFN12 complex. Hydrogen bonds in (F-G) were indicated by red dotted lines.

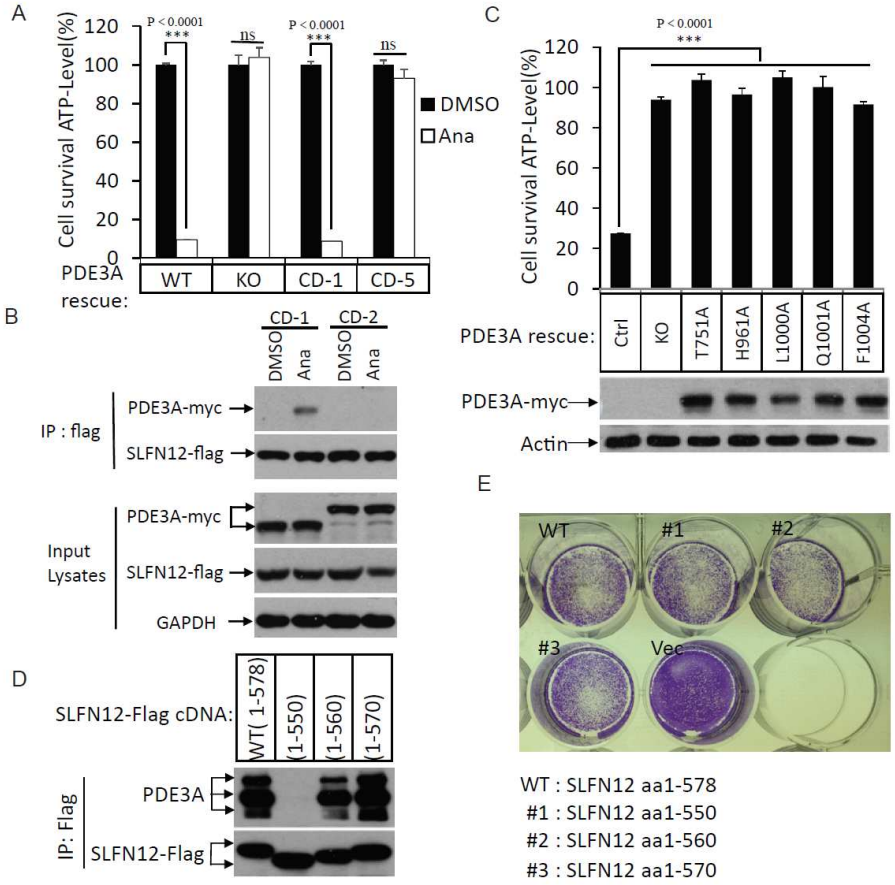

Figure 3. The Anagrelide-induced PDE3A-SLFN12 interaction depends on PDE3A's catalytic domain and SLFN12's C-terminal region.

(A) HeLa (PDE3A$^{-/-}$) clone generated by CRISPR/Cas9 system. PDE3A truncation aa669-1102 (CD-1) and aa679-1141 (CD-2) were stably transfected in HeLa (PDE3A$^{-/-}$) cells. The knockout and rescue cells were treated with the indicated stimuli for 36 hours. Cell viability was determined by measuring ATP levels treated with the indicated stimuli for 36 hours. Cell viability was determined by measuring ATP levels. The data are represented as the mean ± SD of triplicate wells.

(B) PDE3A truncation (CD-1 and CD-2) were stably transfected in HeLa (SLFN12$^{-/-}$)-SLFN12-HA-3×Flag cells. The cells were treated with Anagrelide for 12 hours. SLFN12 was immunoprecipitated using anti-Flag resin. The immunocomplexes and lysates were analyzed by immunoblotting using antibodies as indicated.

(C) The PDE3A (WT) and different site mutants of PDE3A were stably expressed in HeLa (PDE3A$^{-/-}$) cells. The cells were treated with Anagrelide for 36 hours. Cell viability was determined by measuring ATP levels (upper panel). The data are represented as the mean ± SD of triplicate wells. PDE3A expression was measured by anti-Myc immunoblotting (lower panel).

(D) The full-length SLFN12 and truncations (aa1-550, aa1-560, aa1-570) were transient transfected in HeLa (SLFN12$^{-/-}$) cells for 24 hours and then Anagrelide treated for 12h. SLFN12 was immunoprecipitated using anti-Flag resin. The immunocomplexes and lysates were analyzed by

immunoblotting using antibodies as indicated.

(E) The full-length SLFN12 and truncations (aa1-550, aa1-560, aa1-570) were transient transfected in HeLa (SLFN12$^{-/-}$) cells for 72 hours and then cells were stained by methylene blue.

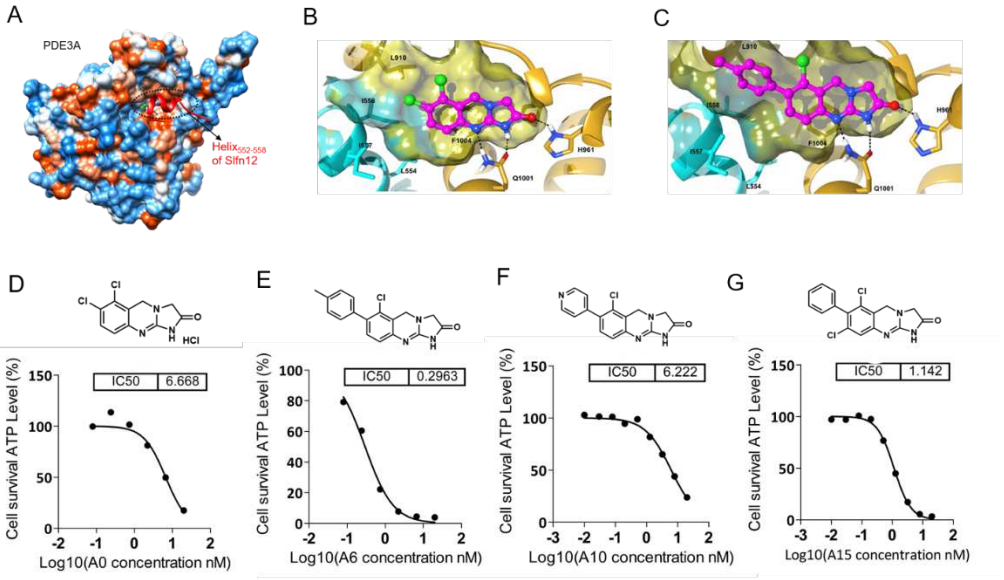

Figure 4 Structure-guided optimization of Anagrelide led to A6 with significant increased activity.

(A) Anagrelide-binding in PDE3A-SLFN12 complex. PDE3A was shown as hydrophobicity surface, colored from orange red (hydrophobic) to blue (hydrophilic). The helix$_{552\text{-}558}$ of SLFN12 was colored in red ribbon.

(B) The interactions of Anagrelide with PDE3A and SFL12. Cyan: SFLN12; yellow: PDE3A, magenta: Anagrelide. The black dash line indicated hydrogen bonds.

(C) The modelled structure of PDE3A-SFL12-A6. Cyan: SFLN12; yellow: PDE3A, magenta: A6. The black dash line indicated hydrogen bonds.

(D-G) HeLa cells were treated with the indicated stimuli for 36 hours. Cell viability was determined by measuring ATP levels. The data are analyzed using GraphPad Prism5.

Figures

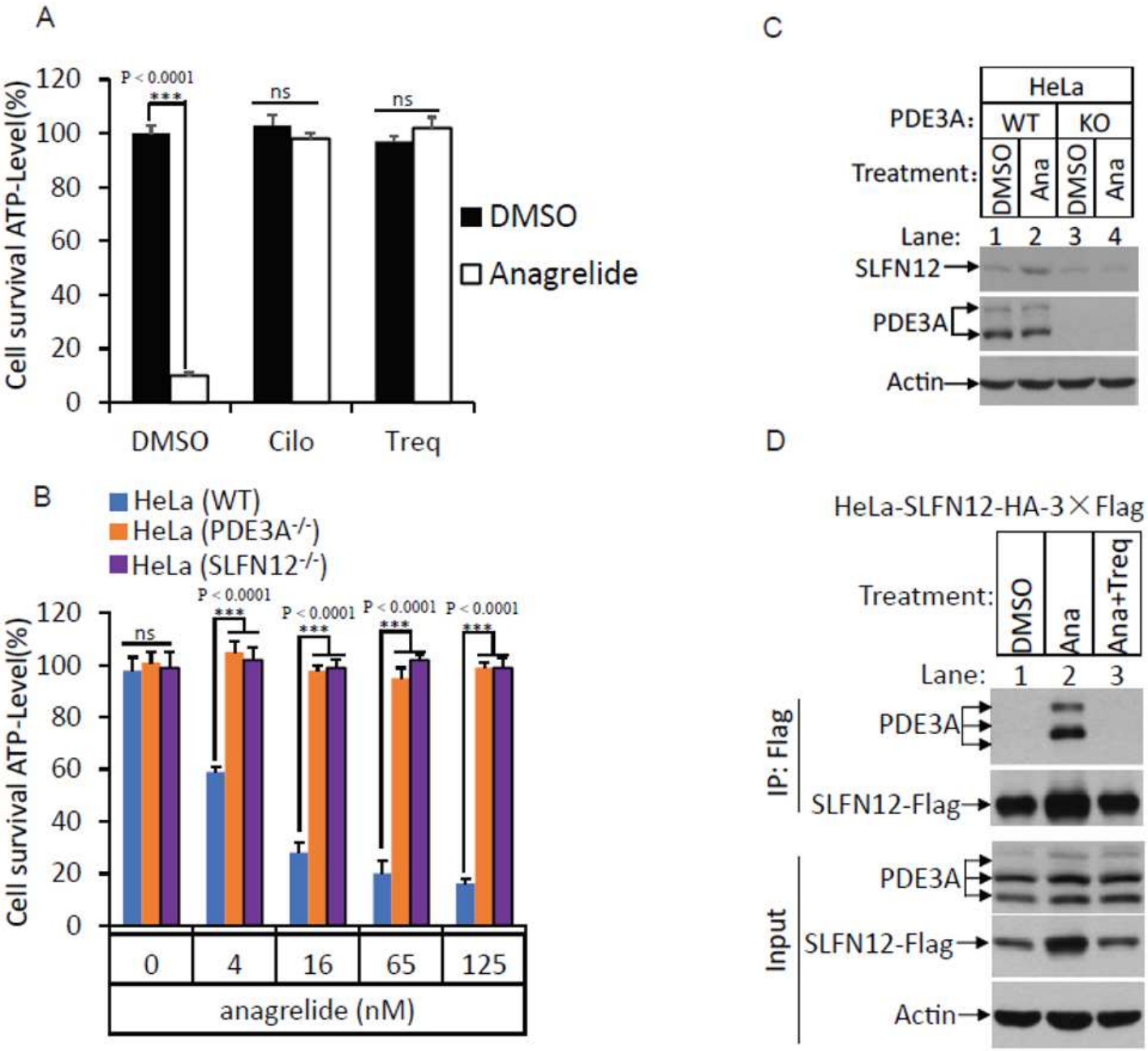

Figure 1

Anagrelide-mediated cell death depends on PDE3A and SLFN12 (A) HeLa cells were treated with the indicated stimuli for 36 hours. Cell viability was determined by measuring ATP levels. The data are represented as the mean ± SD of triplicate wells. Identical concentrations of Anagrelide (100 nM), Cilostazol (1 μM) and Trequinsin (25 nM) were used in subsequent experiments unless otherwise stated. (B) HeLa (WT), HeLa (PDE3A-/-) and HeLa (SLFN12-/-) cells were treated with Anagrelide with the indicated concentration for 36 hours. Cell viability was determined by measuring ATP levels. The data are represented as the mean ± SD of triplicate wells. (C) HeLa (WT and PDE3A-/-) cells were treated with the

indicated stimuli for 12 hours. The lysates were analyzed by immunoblotting using SLFN12 and PDE3A antibody. (D) HeLa-SLFN12-HA-3×Flag cells were treated with the indicated stimuli for 12 hours. SLFN12 was immunoprecipitated using anti-Flag resin. The immunocomplexes and lysates were analyzed by immunoblotting using antibodies as indicated.

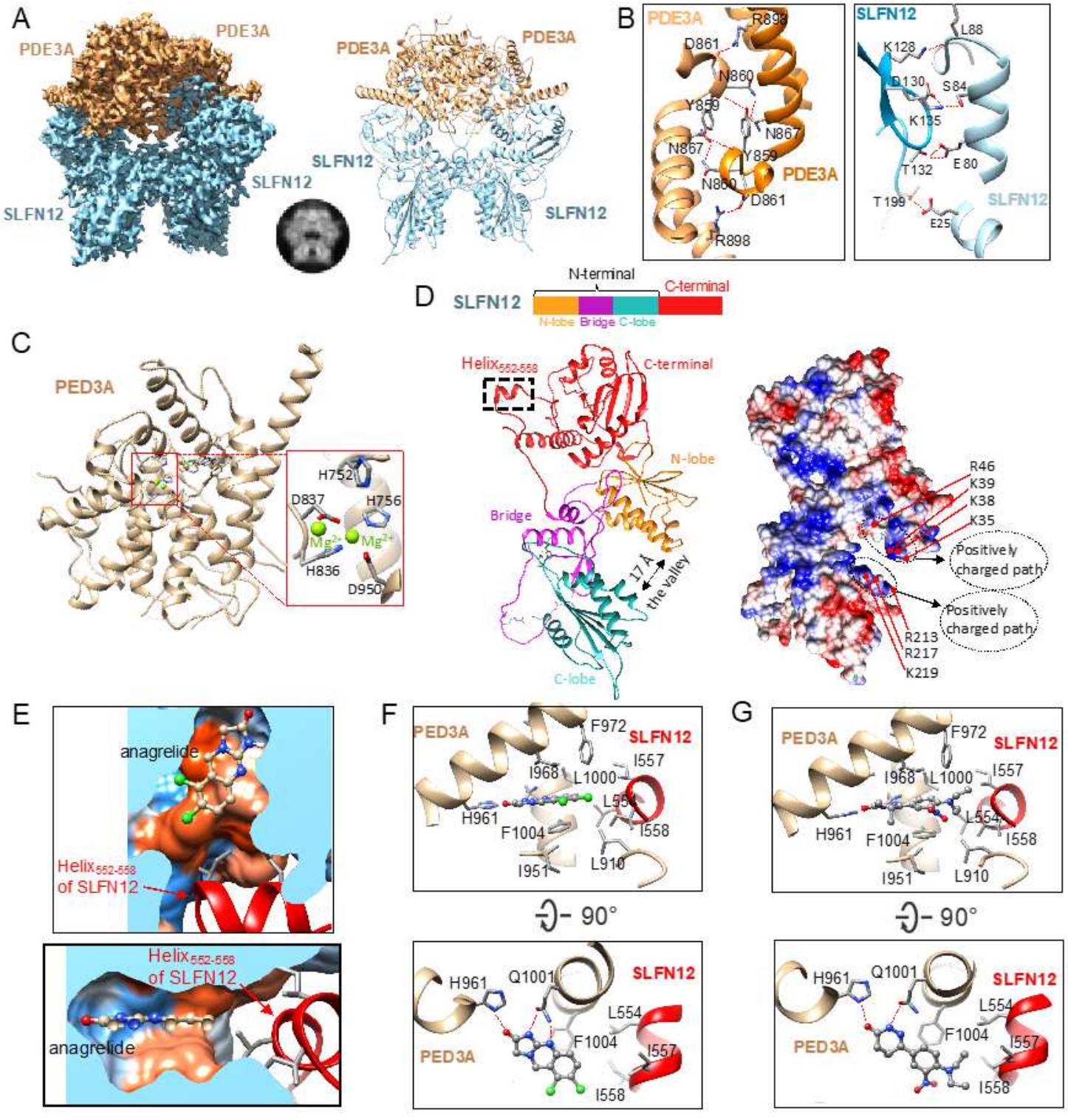

Figure 2

Cryo-EM analysis of Anagrelide- and DNMDP-induced PDE3A-SLFN12 complexes. (A) The cryo-EM reconstruction of Anagrelide-induced PDE3A-SLFN12. Left, the cryo-EM density with PDE3A colored in sandy brown and SLFN12 in light blue. Right, the corresponding atomic model. A selected image from the 2D classification was also displayed, demonstrating the butterfly-like shape. (B) The dimeric interaction interfaces of PDE3A (left) and SLFN12 (right). Hydrogen bonds were labelled by red dotted lines. (C) The model of C terminal of PDE3A. The zoom-in image of Mg2+ ions binding site was indicated by the red box. Residue H752 of PDE3A was folded close to the two Mg2+ ions. (D) Left was the model of SLFN12, divided to two domains, the N-terminal and C-terminal domains. The N-terminal domain consisted of two lobes and a bridge motif, forming a U-shaped valley with a diameter of ~17 Å. Right was the electrostatic surface potentials of SLFN12 in the same view to the left model, colored from red (negative) to blue (positive). The positively charged amino acids located at the valley mouth were indicated, forming two positively charged paths, responsible for RNA binding. (E) Tow zoom-in views of anagrelide-binding pocket in PDE3A-SLFN12 complex. Upper view was parallel to the plane of anagrelide, while the below view was perpendicular to anagrelide plane. PDE3A was shown as hydrophobicity surface, colored from orange red (hydrophobic) to blue (hydrophilic). The helix552-558 of Slfn12 was colored in red ribbon. (F) Anagrelide-binding site in PDE3A-SLFN12 complex. Anagrelide was anchored at the binding pocket by forming hydrogen-bond network with H961 and Q1001 of PDE3A and hydrophobic interaction with helix552-558 of SLFN12. (G) DNMDP-binding site in PDE3A-SLFN12 complex. Hydrogen bonds in (F-G) were indicated by red dotted lines.

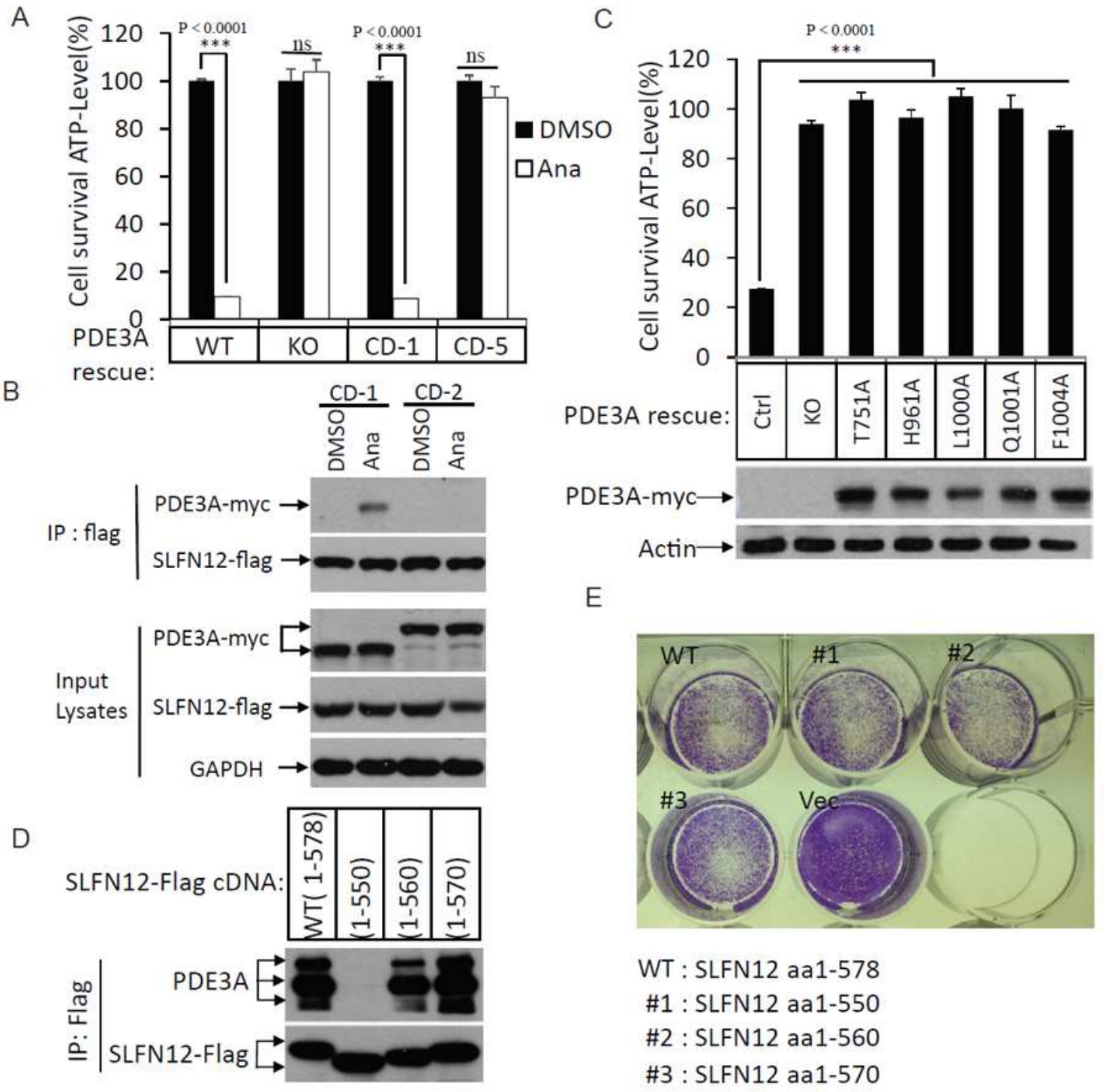

Figure 3

The Anagrelide-induced PDE3A-SLFN12 interaction depends on PDE3A's catalytic domain and SLFN12's C-terminal region. (A) HeLa (PDE3A-/-) clone generated by CRISPR/Cas9 system. PDE3A truncation aa669-1102 (CD-1) and aa679-1141 (CD-2) were stably transfected in HeLa (PDE3A-/-) cells. The knockout and rescue cells were treated with the indicated stimuli for 36 hours. Cell viability was determined by measuring ATP levels treated with the indicated stimuli for 36 hours. Cell viability was determined by measuring ATP levels. The data are represented as the mean ± SD of triplicate wells. (B)

PDE3A truncation (CD-1 and CD-2) were stably transfected in HeLa (SLFN12-/-)-SLFN12-HA-3×Flag cells. The cells were treated with Anagrelide for 12 hours. SLFN12 was immunoprecipitated using anti-Flag resin. The immunocomplexes and lysates were analyzed by immunoblotting using antibodies as indicated. (C) The PDE3A (WT) and different site mutants of PDE3A were stably expressed in HeLa (PDE3A-/-) cells. The cells were treated with Anagrelide for 36 hours. Cell viability was determined by measuring ATP levels (upper panel). The data are represented as the mean ± SD of triplicate wells. PDE3A expression was measured by anti-Myc immunoblotting (lower panel). (D) The full-length SLFN12 and truncations (aa1-550, aa1-560, aa1-570) were transient transfected in HeLa (SLFN12-/-) cells for 24 hours and then Anagrelide treated for 12h. SLFN12 was immunoprecipitated using anti-Flag resin. The immunocomplexes and lysates were analyzed by immunoblotting using antibodies as indicated. (E) The full-length SLFN12 and truncations (aa1-550, aa1-560, aa1-570) were transient transfected in HeLa (SLFN12-/-) cells for 72 hours and then cells were stained by methylene blue.

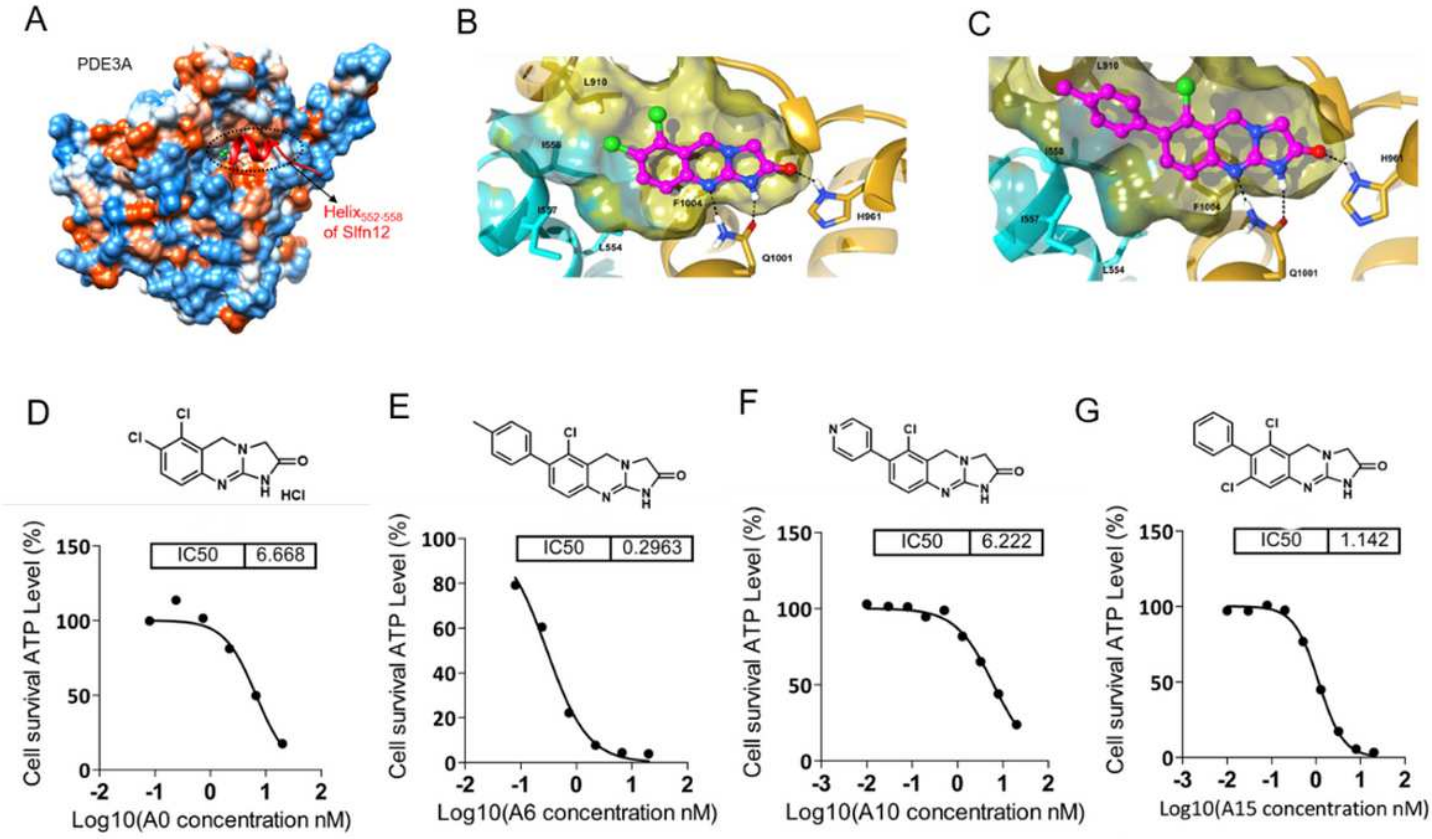

Figure 4

Structure-guided optimization of Anagrelide led to A6 with significant increased activity. (A) Anagrelide-binding in PDE3A-SLFN12 complex. PDE3A was shown as hydrophobicity surface, colored from orange red (hydrophobic) to blue (hydrophilic). The helix552-558 of SLFN12 was colored in red ribbon. (B) The interactions of Anagrelide with PDE3A and SFL12. Cyan: SFLN12; yellow: PDE3A, magenta: Anagrelide. The black dash line indicated hydrogen bonds. (C) The modelled structure of PDE3A-SFL12-A6. Cyan: SFLN12; yellow: PDE3A, magenta: A6. The black dash line indicated hydrogen bonds. (D-G) HeLa cells

were treated with the indicated stimuli for 36 hours. Cell viability was determined by measuring ATP levels. The data are analyzed using GraphPad Prism5.

Supplementary Files

This is a list of supplementary files associated with this preprint. Click to download.

- SupplementalInformation.pdf